SECONDARY SHEAR WAVES FROM SOURCE BOREHOLES

by

J.A. Meredith, C.H. Cheng and M.N. Toksöz

Earth Resources Laboratory
Department of Earth, Atmospheric, and Planetary Sciences
Massachusetts Institute of Technology
Cambridge, MA 02139

ABSTRACT

The purpose of this paper is to synthesize the most important results of the thesis work of Meredith (1990) concerning radiation from seismic sources in boreholes.

Previous studies of radiation from sources in boreholes have been far-field studies and have neglected the explicit contribution of the borehole. In general, this is fine for P-wave radiation and for S-wave radiation into high velocity rocks. However, tube waves "leak" shear conical waves (Mach waves) which propagate when the tube wave velocity is greater than the shear wave velocity of the surrounding medium. These Mach waves are of high amplitude because of the dominance of the tube wave and radiate away from the borehole in a fixed conical shape. The shape of the cone is dependent on the shear wave velocity of the medium and the tube wave velocity.

This paper defines the conditions under which these Mach waves exist and thoroughly describes them in a physical sense and less so in a mathematical sense. Finally, the relationship of Mach waves to data sets is examined and how Mach waves may be confused with receiver borehole tube waves. To keep the presentation simple, radiation from axial or torsional sources or radiation from empty boreholes is omitted in this paper but fully addressed in Meredith (1990).

INTRODUCTION

For the most part, analysis of cross well tomographic data has resulted in travel time picks which are inverted based on a forward velocity model. This produces a P-wave velocity image of the region between the two wells. However, there is also interest in determining amplitudes and determining S-wave velocities in addition to the P-wave velocities.

To accomplish these expanded goals, understanding of the total wavefield radiated by a seismic source in a borehole is required. Radiation from seismic sources in a borehole has been developed through Lee and Balch's work (Heelan 1953a; Lee and Balch, 1982; Winbow, 1989) describing far-field radiation from a point source or radial source in a fluid-filled borehole. By assuming the far-field and the mathematical simplifications that implies, closed form solutions for far-field radiation can be achieved based on simple trigonometric functions. These functions can be graphed producing a radiation pattern such as presented in Figure 1 for a point source in a fluid-filled borehole.

Following these theoretical developments, experiments have been run to test their validity in practice. White and Sengbush (1963) published the result of an experimentally determined radiation pattern versus the theoretical prediction. The experiment was conducted in the relatively homogeneous and massive Pierre Shale. A schematic of the experiment is outlined in Figure 2 where it can be seen that in a central shot hole drilled 600' below the surface, booster charges are fired and the resulting radiation is recorded by six 3 component geophones in receiver boreholes. The receiver boreholes were drilled in a circular pattern to represent one quadrant of a radiation pattern. The resulting data versus the radiation pattern prediction from Heelan (1953) is shown as Figure 3 (White and Sengbush, 1963). It is immediately apparent from Figure 3 that there is substantial disagreement between the theoretical prediction and the actual data. In particular, the radiation pattern prediction fails to account for the strong vertical directivity of the shear wave amplitude. White and Sengbush surmised that the difference was that Heelan's empty borehole theory could not account for the effects of tube waves present in the experiment. But at a later time, Fehler and Pearson (1984) performed a similar type experiment (Figure 4) in granite and found good agreement with their data and the radiation pattern prediction.

Therefore, this work was carried out to resolve this type of discrepancy — radiation pattern predictions work in high velocity reservoirs but seemingly fail in low velocity reservoirs for shear wave amplitude predictions.

DEVELOPMENT OF A NUMERICAL SOLUTION

The first effort of this work was to develop a full numerical technique to see if a numerical solution could reproduce the behavior of the data. To do so a program to calculate the radial and vertical displacements outside a radially layered medium was developed. This effort is complementary to that of Tubman (1984), and Tubman et al. (1984, 1986) who studied the pressure response inside a layered medium using a discrete wavenumber Thomson-Haskell approach. A numerical refinement to the Tubman et al. work for calculating the layer matrices (Schmitt and Bouchon, 1985) was also incorporated into this work. In essence, the work of Tubman et al. was turned inside out for a complete numerical solution and was tested against a boundary integral code (Meredith, 1990)

and yielded identical results. More details of the algorithm can be found in the Tubman et al. references, Meredith (1990), or Meredith et al. (1990).

RESULTS OF NUMERICAL MODELLING

In general, there was excellent agreement between the theoretical prediction of P-wave radiation and the numerical prediction even less than 1 m away from the borehole. Thus for P-wave radiation the far field assumptions are quite valid. There is also excellent agreement between theoretical and numerical predictions of S-wave behavior if the S-wave velocity of the surrounding medium is fairly high ($V_s >> V_f$) (Meredith, 1990). Conversely, the numerical prediction diverged from the theoretical but agreed quite well with the experimental observations when the shear wave velocity was close to or less than the tube wave velocity.

For example, Figure 5 is a polar plot displaying White and Sengbush's observed data versus the numerical model predictions. The strong vertical directivity of the shear wave amplitude is very well duplicated and the numerical model represents a substantial improvement over the theoretical prediction in Figure 4.

The reason for the improvement by using the numerical model is that the numerical solution includes the effects of the tube wave travelling in the borehole whereas the far-field solution does not. As predicted by White and Sengbush (1963) and de Bruin and Huizer (1989), the tube wave has a direct affect on the radiation. The mechanism describing how tube wave propagation affects the radiation into the borehole is discussed in physical and mathematical terms next.

PHYSICS OF TUBE WAVE RADIATION: THE MACH WAVE

Constructive and destructive interference due to superposition of wavefields is one of the fundamental principles of wave theory. It similarly plays a large role in describing how a tube wave radiates shear conical waves (Mach waves) into the surrounding medium.

In cased boreholes, Tubman et al. (1984) and Winbow (1989) had shown that less than 1% of the source's energy escapes into the formation while the remainder is trapped in the tube waves. Tube waves radiate sound into the formation as they travel through the borehole and in fact one of the conditions for their existence (Cheng and Toksöz, 1981) is that they radiate this energy. However, the energy decays away from the borehole. When the tube wave velocity exceeds the shear wave velocity the radiated noise overlaps and in fact constructively interferes (de Bruin and Huizer, 1989). This phenomenon is most closely related to that encountered in aerodynamics and is illustrated

by Figure 6. In the sub-shear case sound emitted by the tube wave decays away from the borehole in a spherical fashion as in the top half of Figure 6. In the super-shear case, sound emitted by the tube wave does overlap causing constructive interference. When this sound overlaps, the cone of constructive interference is determined by an angle, the Mach angle, whose sine is the ratio of shear wave velocity over tube wave velocity. One note is that the Mach angle is measured from the axis of the cone. The Mach number is the ratio of tube wave velocity over the shear wave velocity and is greater than one when Mach waves exist.

To illustrate this phenomenon of constructive interference, some models were run with high and low velocity media surrounding the borehole. The source was a 200 Hz Ricker wavelet. Radial and vertical displacements were calculated on a 50m by 50m grid at half meter intervals with the source location being the origin. Total displacement was derived from the radial and vertical displacements and the result was contoured. These displacement fields were then sampled at a particular time to produce a snapshot, analogous to the procedure commonly performed in finite difference calculations.

The first model is the counter example, the high velocity case, which uses the velocities and densities (Table 1) of Berea Sandstone for the surrounding medium. The borehole was open and the contour plot of the displacements at 20 msecs is shown in Figure 7A. The P wave has moved off the graph and the S wave and tube wave are contoured. It can be seen that the tube wave response dies off with distance away from the borehole and there is no constructive interference of the sound emitted from the tube wave. This is the sub-shear case because the tube wave velocity at 1400 m/sec is less than the shear wave velocity of 2664 m/sec. Stepping in time to 30 msecs, Figure 7B, shows no real difference, there is still no constructive interference of the tube wave and the tube wave radiation shape is identical.

The second model uses the physical properties of Pierre Shale (Table 1), a much slower medium and the medium used by White and Sengbush (1963). This is the supershear case because the tube wave velocity of 980 m/sec is greater than the shear wave velocity of 869 m/sec. The contour plot at 20 msecs, Figure 8A, shows a P and S wave but it can be seen that the borehole side of the S wave is due to constructive interference of the tube wave and is of high amplitude. The Mach angle here is relatively steep at 63 degrees.

The third model (Figure 9) is the same as for Figure 8 but now a 0.5 cm layer of casing has been inserted raising the tube wave velocity to 1280 m/sec using the formulas of Marzetta and Schoenberg (1985) and changing the Mach angle to 43 degrees. The P wave is only slightly affected by the presence of the casing. By changing the Mach angle, direct detection by a vertical array of receivers is even more likely.

The geometric shape of the S-wave radiation when the Mach wave is present is due to the constructive interference and consists of the initial disturbance plus the

constructively interfering Mach wave. The initial disturbance will not experience any constructive or destructive interference until the tangent of the Mach cone intersects this disturbance as shown in Figure 10 at the angle ϕ_c. The portion of the medium illuminated by the Mach wave is said to be in the Mach cone. Therefore, the shape of the radiated wave field will have an outwardly travelling spherical portion tangent to an upgoing and downgoing Mach cone. The Mach wave will directly intersect any geophone in the Mach cone and may indirectly intersect other geophones through reflections of Mach waves. The spherical portion inside the Mach cone will be destroyed by destructive interference.

When an observation point is inside the Mach cone, the arrival time of the Mach wave will be a hybrid travel time as shown in Figure 11. The travel time will consist of the time to travel up the borehole as a tube wave and time to travel through the medium at the shear wave velocity. The hybrid travel time is given by the formula

$$\frac{z}{C_T} + \frac{r\sqrt{M^2-1}}{C_T} \ ,$$

analogous to that from earthquake seismology (Ben-Menahem and Singh, 1987). What this means is that for a vertical array of receivers the moveout will be controlled by the tube wave velocity exclusively and so will be linear. Therefore, a Mach wave may look like a high amplitude receiver borehole tube wave though it is not.

MATHEMATICS OF TUBE WAVE RADIATION

Another way to visualize this is mathematically. The radiation integrals for an infinite half-space surrounding a borehole are typically evaluated by the method of stationary phase (Lee and Balch, 1982; Winbow, 1989; Meredith, 1990).

Using the method of stationary phase implies that the most significant contribution to the integral occurs in the neighborhood of a stationary point where the integral is slowly varying. Away from this point the integral is highly oscillatory and positive and negative oscillations cancel each other.

The integrals of concern here have a pole at $\frac{\omega}{C_T}$ and a branch point at $\frac{\omega}{v}$ where v is either α, P-wave velocity or β, S-wave velocity. A commonly used path of integration for evaluating these stationary phase integrals is displayed in Figure 12 for the P-wave case. In Figure 12, the stationary point ranges from z/R=0 to z/R=1 and consequently the stationary point ranges from 0 to $\frac{\omega}{\alpha}$. The stationary point does not come too close to the tube wave pole in a normal velocity setting. However, if the tube wave velocity is close to the P-wave velocity or greater than the tube wave velocity the pole will have an effect. This situation would be rare with P-wave velocities but in the case of shear

waves it is much more common that the shear wave velocity is less than the tube wave velocity as illustrated in Figure 13.

The sub-shear case, the top half of Figure 13, is very similar to the P-wave case. If $\beta > C_T$ no Mach wave will be produced though as β approaches C_T the shear wavefield will be more substantially affected (Meredith, 1990). The super-shear case involves the presence of Mach waves. Here the stationary point will intersect the pole location at $\frac{\omega}{C_T} = \frac{\omega z}{R\beta}$ for some value of $\frac{z}{R}$. This will make the stationary phase assumptions no longer valid for evaluation of the integral. The mathematics is echoing the point of the physics that when $C_T > \beta$ the borehole can no longer be ignored and the far-field assumptions fail.

MACH WAVES IN DATA SETS

The presence of Mach waves and their effects has already been demonstrated for the White and Sengbush (1963) data set and their effects can also be seen on the data of de Bruin and Huizer (1989) which is shown in Meredith (1990).

One final figure will show the pervasiveness of the Mach waves. Figure 14 shows data from a recent group shoot taken at Texaco's Humble test site. The vertical component of shot gathers with identical geometries but different sources are shown. Nice P-wave hyperbolas are evident but none are seen for the S waves. Strong linear events are seen for both the dynamite and airgun experiments. It might first be thought these are receiver borehole tube waves but because the receiver array was cemented and there is no receiver borehole this is impossible. Instead these are Mach waves, and as mentioned before the moveout is linear at the tube wave velocity. Since the dynamite forces the formation nonlinearly, it puts more energy into the formation and comparatively less into the tube wave. Therefore, the Mach wave response for the dynamite is less.

CONCLUSIONS

In some cases, the energetic tube waves in the borehole lead to direct radiation of shear conical waves or Mach waves into the surrounding formation. However, P-wave radiation is not substantially affected by the presence of the borehole. The existence of these Mach waves is dependent on the shear wave velocity of the medium being less than the tube wave velocity. The Mach waves will be controlled by a Mach cone and an angle whose sine is the ratio of the shear wave velocity over tube wave velocity. The travel time to a receiver in the Mach cone will be a hybrid travel time and will include travel time as a tube wave and as a shear wave in the formation. The distinction between an observation point being inside the Mach cone or outside depends on the tube wave and

shear wave velocity.

The Mach wave phenomenon has been noticed in data sets such as White and Sengbush (1963), de Bruin and Huizer (1989), and in a recent group shoot at the Texaco Humble test site. Included in these data sets have been buried receiver arrays which preclude the presence of receiver borehole tube waves thus removing ambiguity.

ACKNOWLEDGMENTS

We would like to thank Ari Ben-Menahem, Michel Bouchon, Luc Boelle, Benoit Paternoster, and Roger Turpening for valuable discussions and Jim DiSiena and Benoit Paternoster for suggesting the topic. This work was supported by the Full Waveform Acoustic Logging Consortium at M.I.T.

Table 1. Physical properties of lithologies and steel casing used in this paper. Velocities in m/sec, densities in kg/m^3.

Lithology/Property	V_p	V_s	ρ	C_T
Berea Sandstone	4206	2664	2140	1400
Pierre Shale	2074	869	2250	980
Steel (Casing)	5940	3228	6268	

REFERENCES

Ben-Menahem, A., and S. Singh, 1987, Supershear accelerations and Mach-waves from a rupturing fault Part I. Theoretical model and implications, *J. Phys. Earth, 35,* 347–365.

de Bruin, J., and W. Huizer, 1989, Radiation from waves in boreholes, *Scientific Drilling, 1,* 3–10.

Fehler, M., and C. Pearson, 1984, Cross-hole seismic surveys: applications for studying subsurface fracture systems at a hot dry rock geothermal site, *Geophysics, 49,* 37–45.

Heelan, P., 1953, Radiation from a cylindrical source of finite length, *Geophysics, 18,* 685–696.

Lee, M., and A. Balch, 1982, Theoretical seismic wave radiation from a fluid-filled borehole, *Geophysics, 47,* 1308–1314.

Marzetta, T., and M. Schoenberg, 1985, Tube waves in cased borehole, in *SEG Annual Meeting Expanded Technical Program Abstracts.*

Meredith, J., 1990, *Numerical and Analytical Modelling of Seismic Sources: the Near and far field,* Sc.D. Thesis, M.I.T., Cambridge, MA.

Meredith, J., M.N. Toksöz, and C.H. Cheng, 1991, Secondary shear waves generated from source boreholes, *53rd EAEG Meeting,* in press.

Schmitt, D., and M. Bouchon, 1985, Full-wave acoustic logging-synthetic microseismograms and frequency-wavenumber analysis, *Geophysics, 50,* 1756–1778.

Tubman, K.M., 1984, *Full Waveform Acoustic Logs in Radially Layered Boreholes,* Ph.D. Thesis, M.I.T., Cambridge, MA.

Tubman, K.M., C.H. Cheng, and M.N. Toksöz, 1984, Synthetic full-waveform acoustic logs in cased boreholes, *Geophysics, 49,* 1051–1059.

Tubman, K.M., C.H. Cheng, S. Cole, and M.N. Toksöz 1986, Synthetic full-waveform acoustic logs in cased boreholes II. Poorly bonded casing, *Geophysics, 51,* 902–913.

White, J., and R. Sengbush, 1963, Shear waves from explosive sources, *Geophysics, 28,* 1101–1119.

Winbow, G., 1989, Seismic sources in open and cased boreholes, in *SEG Annual Meeting Expanded Technical Program Abstracts.*

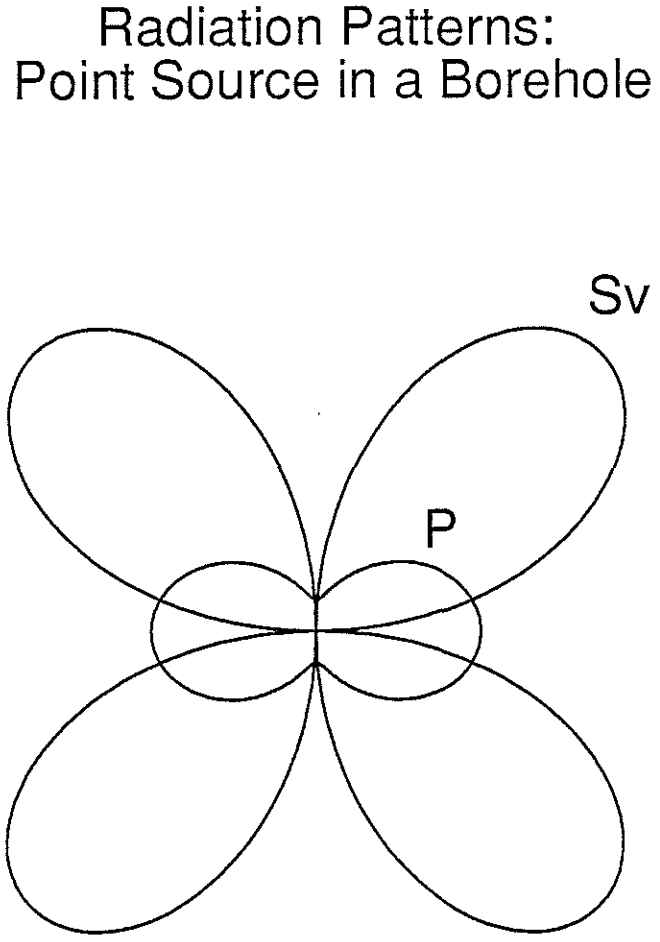

Figure 1: P- and S-wave radiation patterns for a point source or radial source in a borehole. Patterns are essentially identical for an empty borehole (radial source only, Heelan, 1953) or a fluid-filled borehole (Lee and Balch, 1982).

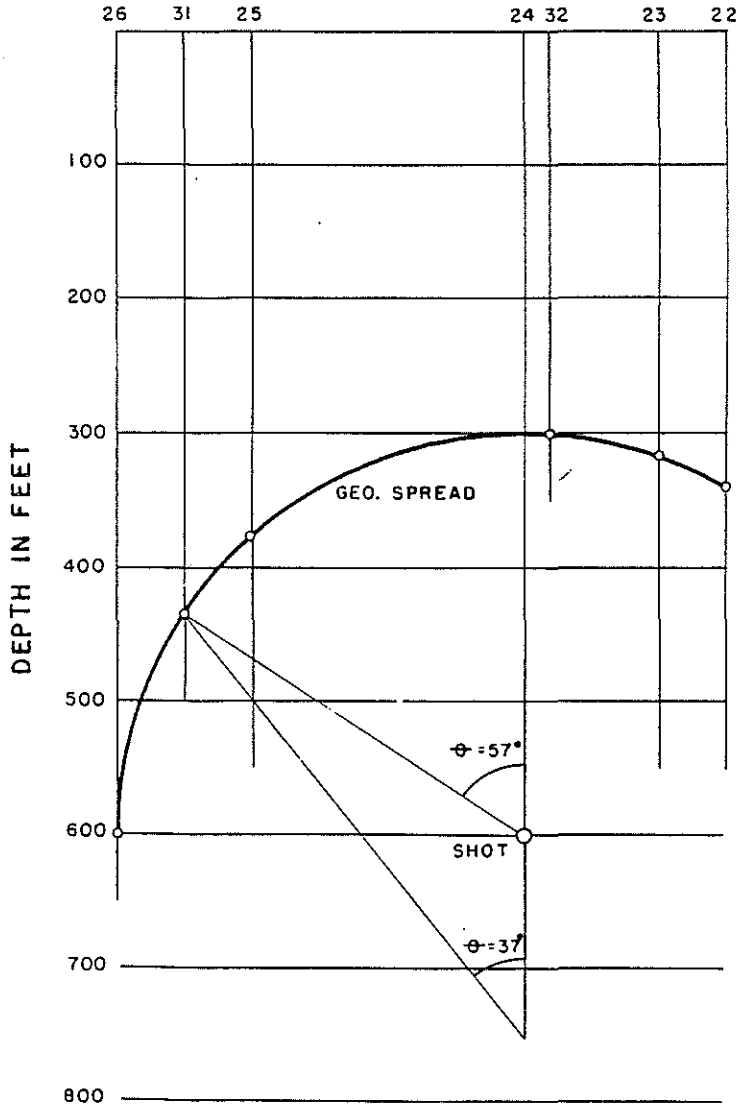

Figure 2: Schematic of experiment by White and Sengbush (Figure 1, 1963). Six receiver boreholes were drilled in a semi-circular arc in a vertical plane including the source borehole (#24). The shotpoint was at 600 ft. depth in the source boreholes. Both source and receiver boreholes were open holes and fluid-filled and the receivers were three component geophones.

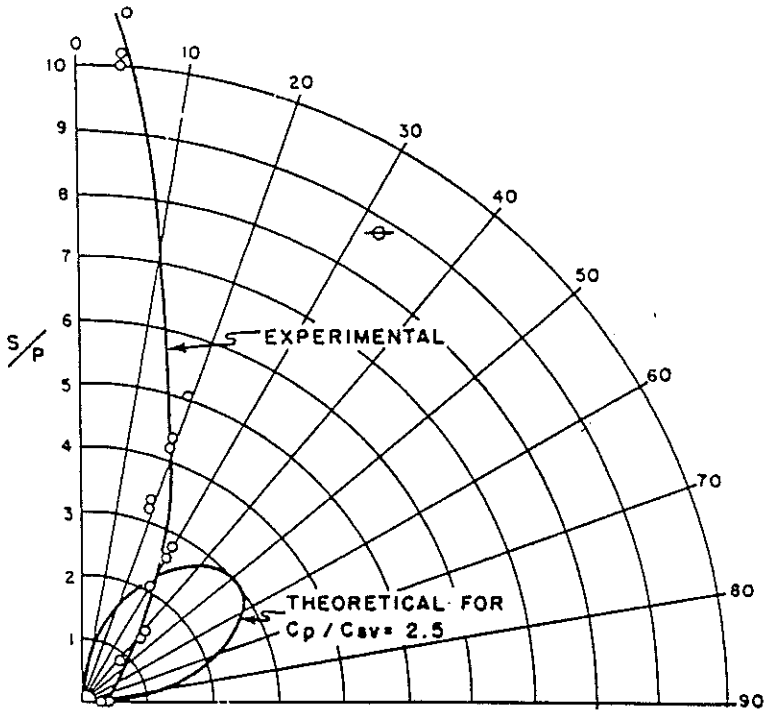

Figure 3: Figure 6 from White and Sengbush (1963). Results of experiment to test Heelan's radiation pattern prediction. Radial axis is S-wave to P-wave amplitude ratio that Heelan's theoretical prediction fails to account for. The experimental data show a strong directivity of S-wave amplitudes. Heelan's theory was for dry boreholes so White and Sengbush surmised that the difference was due to the effects of tube waves which was correct.

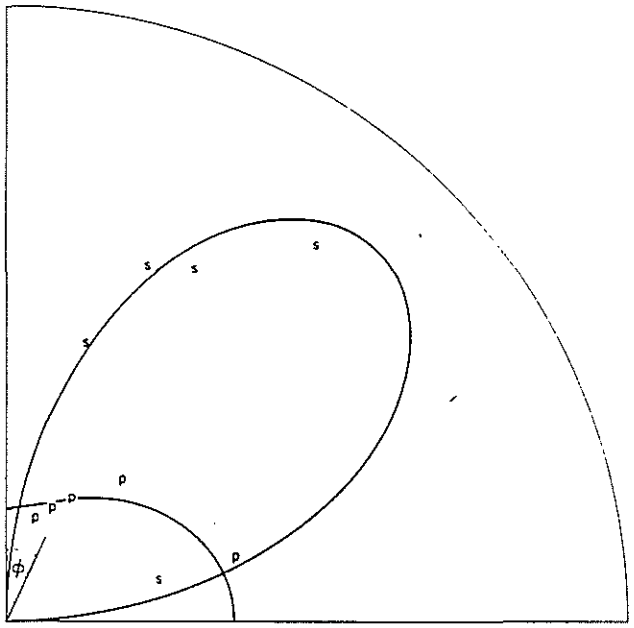

Figure 4: Figure 1 from Fehler and Pearson (1984) showing agreements between experimental data taken in granite and one quadrant of the rose petal shape radiation pattern and peanut shaped P-wave radiation pattern. These independently derived radiation patterns are equivalent to Heelan's (1953).

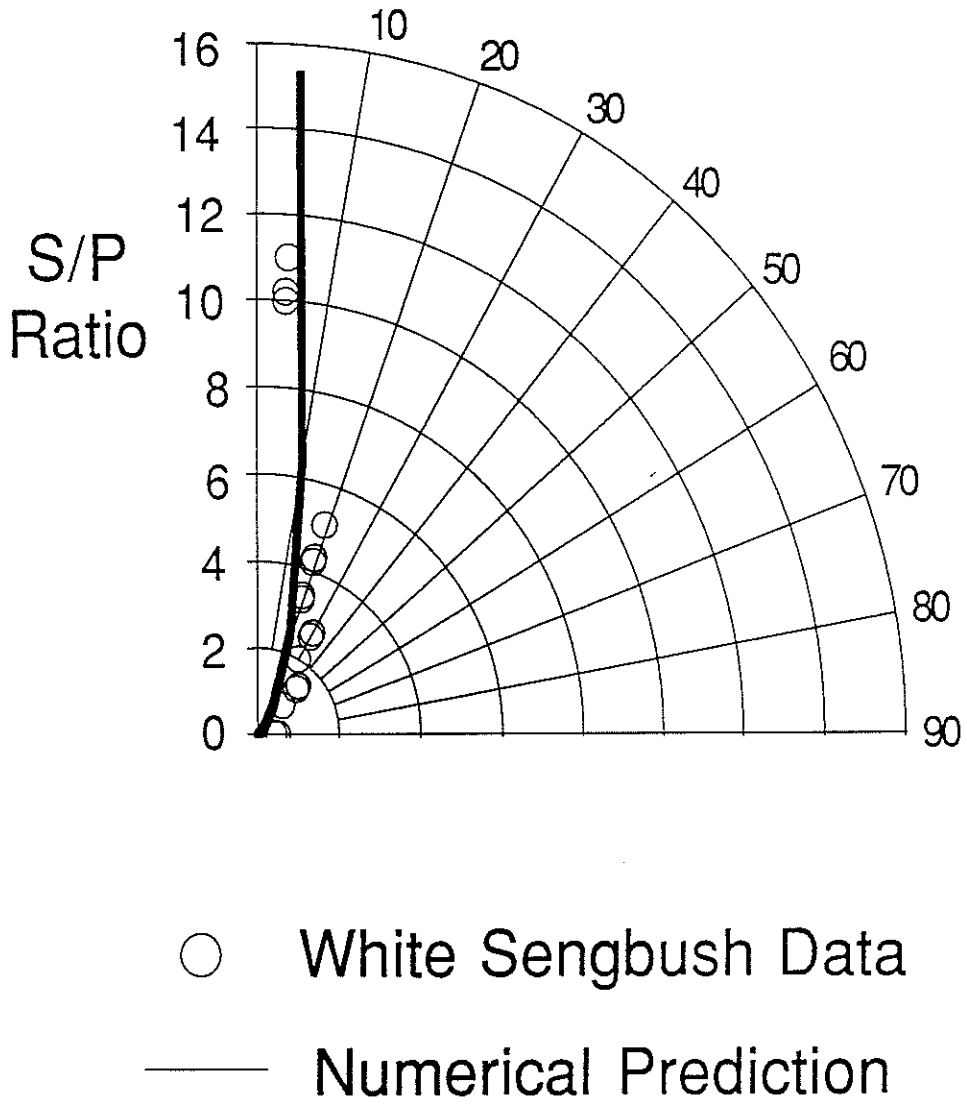

Figure 5: Polar plot displays ratio of S- over P-wave amplitude in Pierre Shale versus co-latitude of station. Data points are from Figure 6 (White and Sengbush, 1963) and Figure 3. When compared to Figure 3 it can be seen with the numerical solution the vertical skewness has been reproduced and much better agreement is seen.

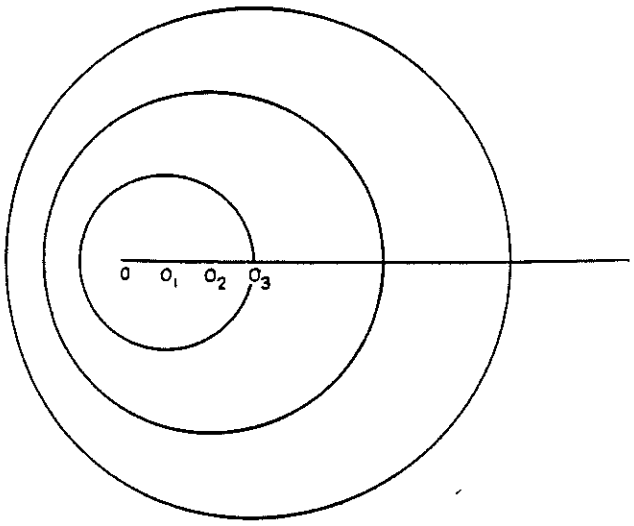

FIG. 1.

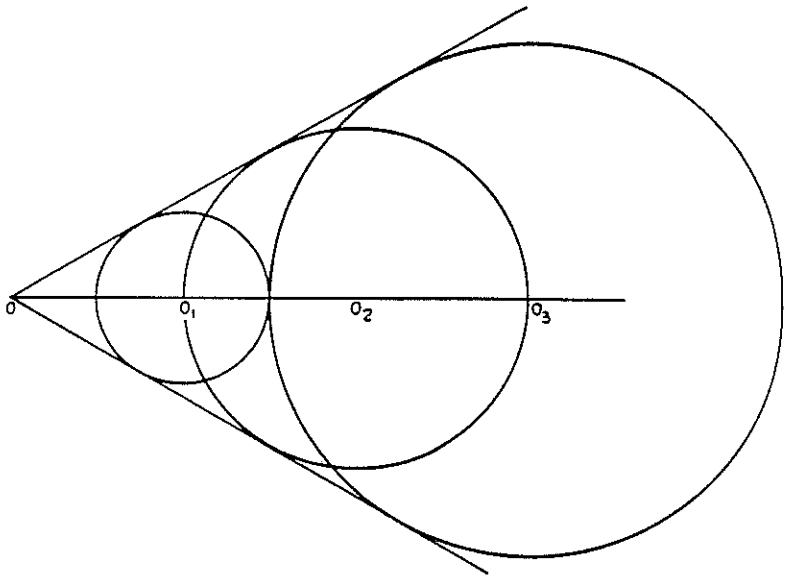

FIG. 2.

Figure 6: Figure from aerodynamics textbook. Top half shows an analog to the sub-shear case where the tube wave velocity is less than the shear wave velocity. Here radiation (spheres) emitted from the tube wave at the tube wave velocity does not overlap before it travels away from the borehole at compressional and shear wave velocities. The bottom half shows the analog to the super-shear case. Here radiation emitted from the tube wave does constructively interfere before travelling at shear wave velocity. This causes a Mach wave and the sine of the angle of the cone from the vertical is equal to the ratio of shear wave velocity over tube wave velocity. Similar to a figure presented by de Bruin and Huizer (1989).

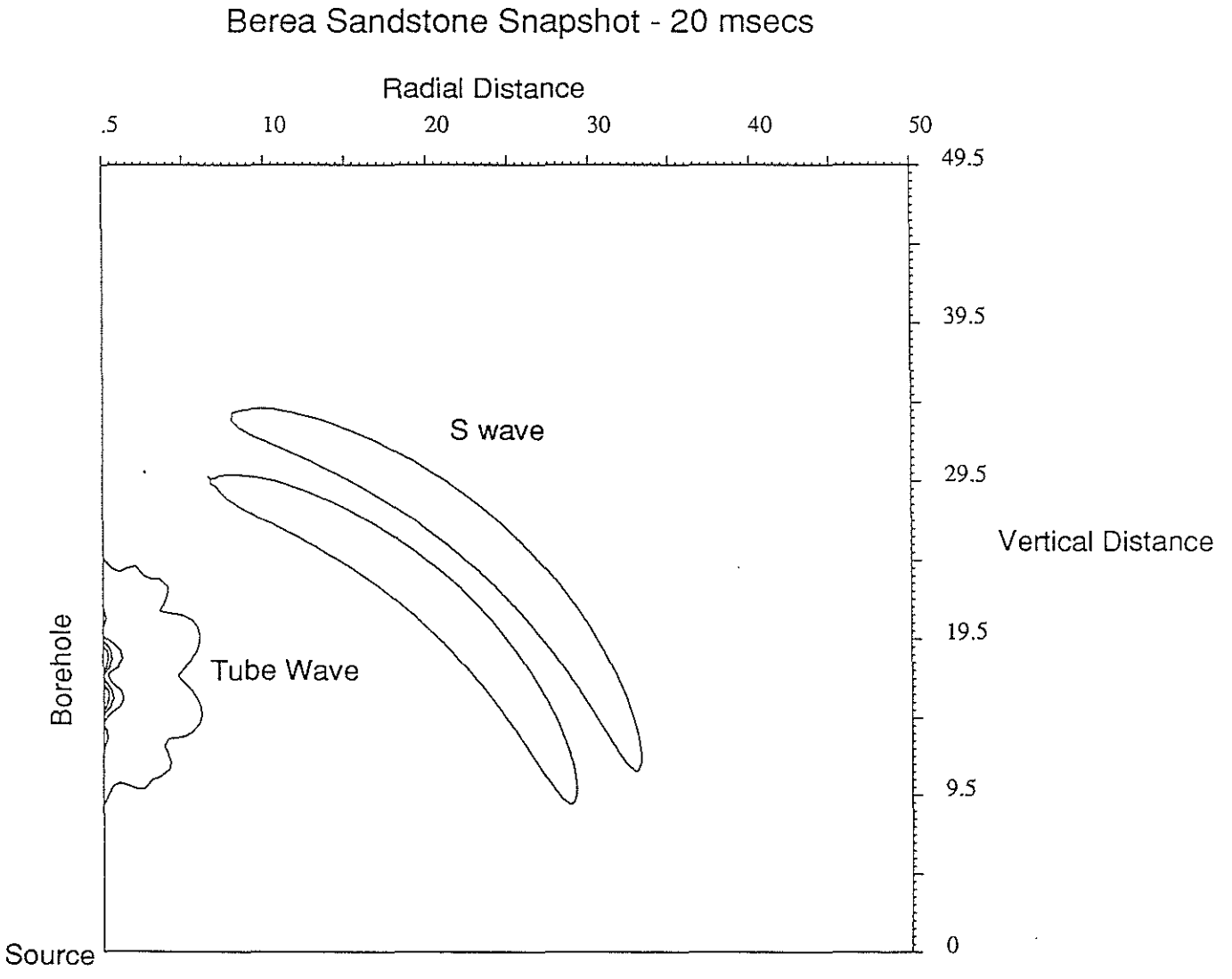

Figure 7: A) A snapshot at 20 msecs of total displacement calculated on a 50 m by 50 m grid and contoured. Origin is source point in lower left hand corner. Velocities and densities for this model are those of Berea Sandstone. P wave is off the grid by this time. Notice tube wave emitting energy but no constructive interference is evident. 200 Hz Ricker wavelet. Contours: minimum 5×10^{-6}, maximum 1.005×10^{-3}, interval 2×10^{-4}.

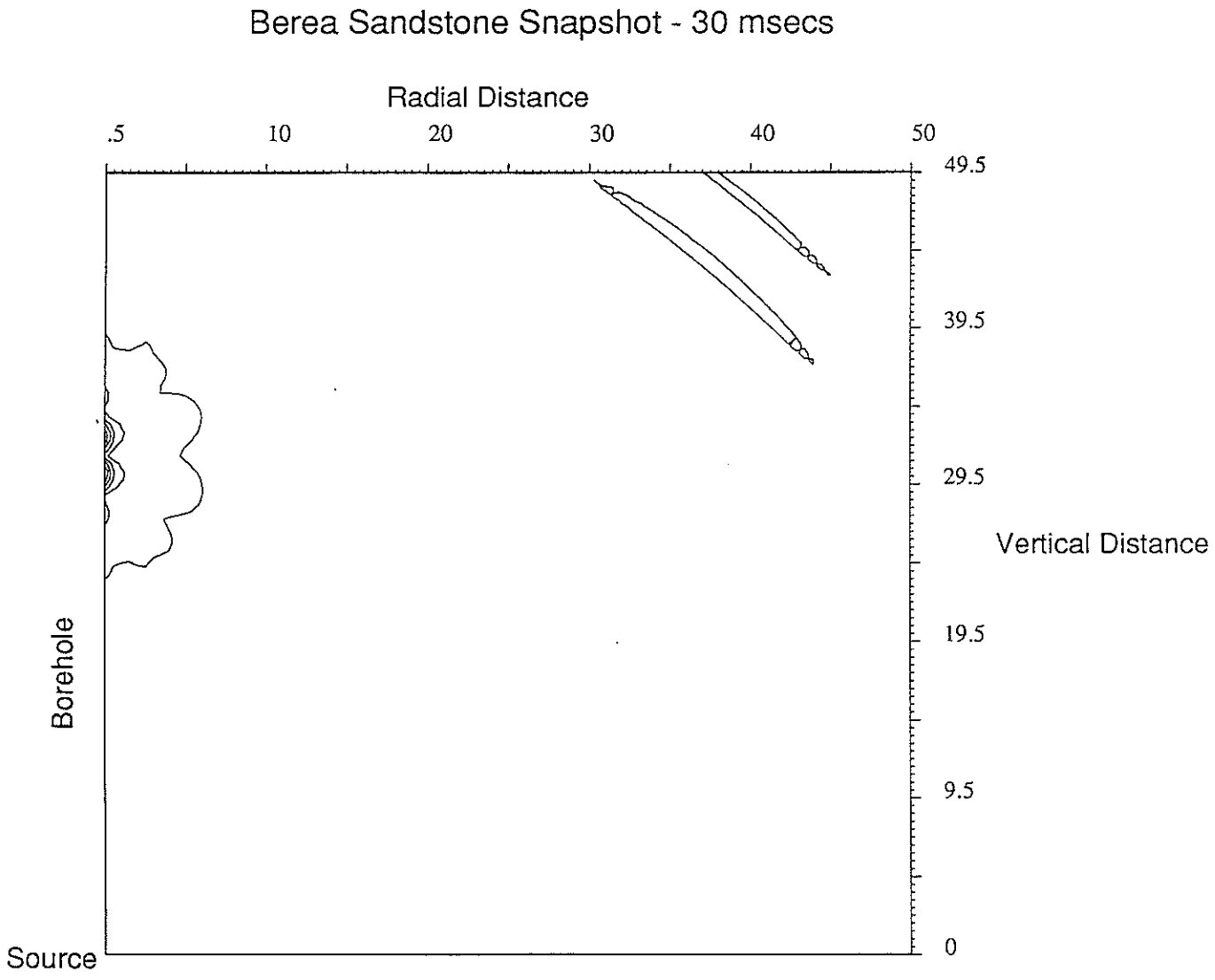

Figure 7: B) A snapshot at 30 msecs of total displacement calculated on a 50 m by 50 m grid and contoured. Same model as part A. Notice shape of tube wave radiation is unchanged from part A.

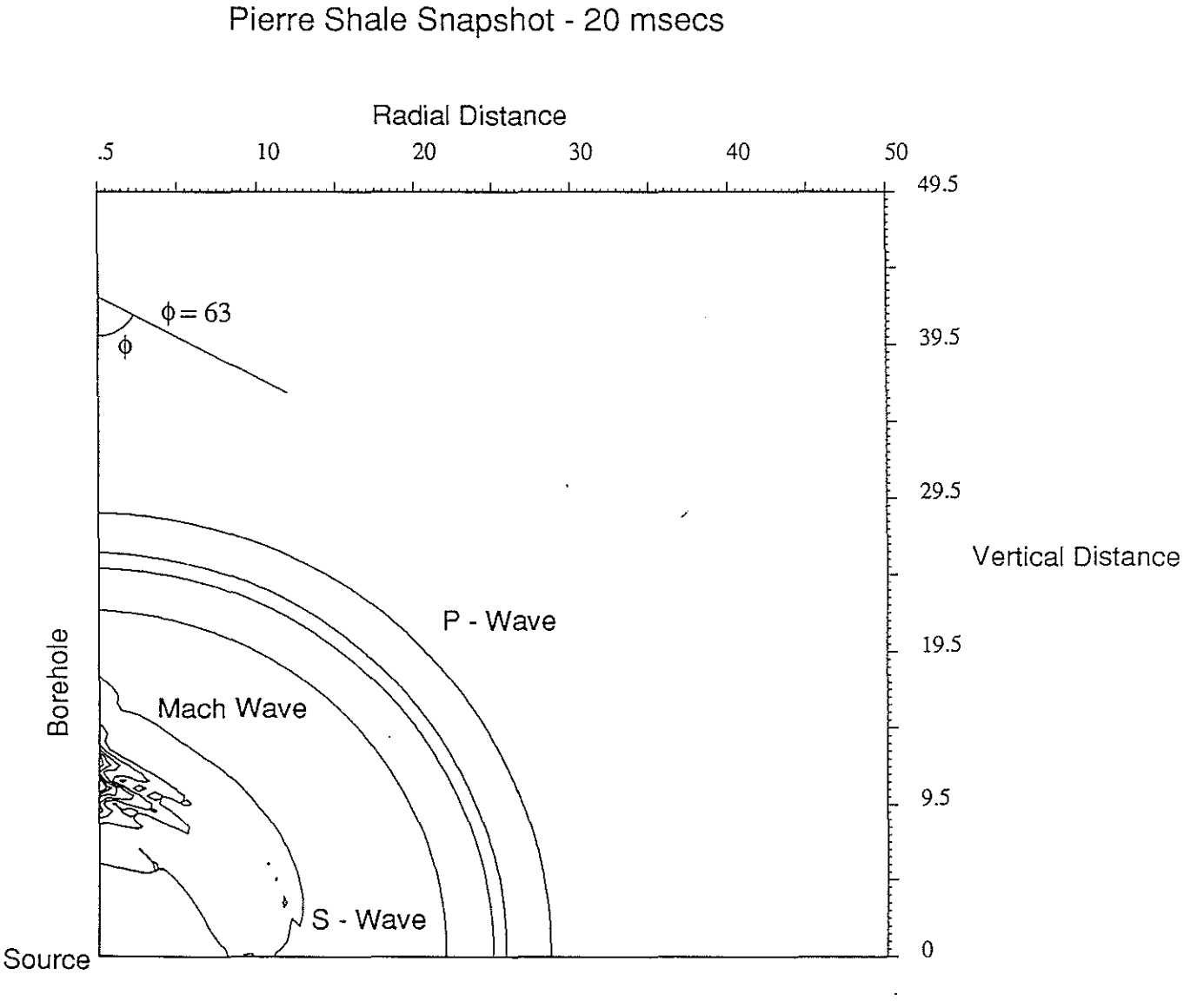

Figure 8: A) A snapshot at 20 msecs of total displacement calculated on a 50 m by 50 m grid and contoured. Origin is source point in lower left hand corner. Velocities and densities for this model are those of Pierre Shale. Notice tube wave emitting energy that is constructively interfering. 200 Hz Ricker wavelet. Contours: minimum 2×10^{-5}, maximum 7×10^{-3}, interval 1×10^{-3}. ϕ is the Mach angle equal to the sine of the shear wave velocity over the tube wave velocity.

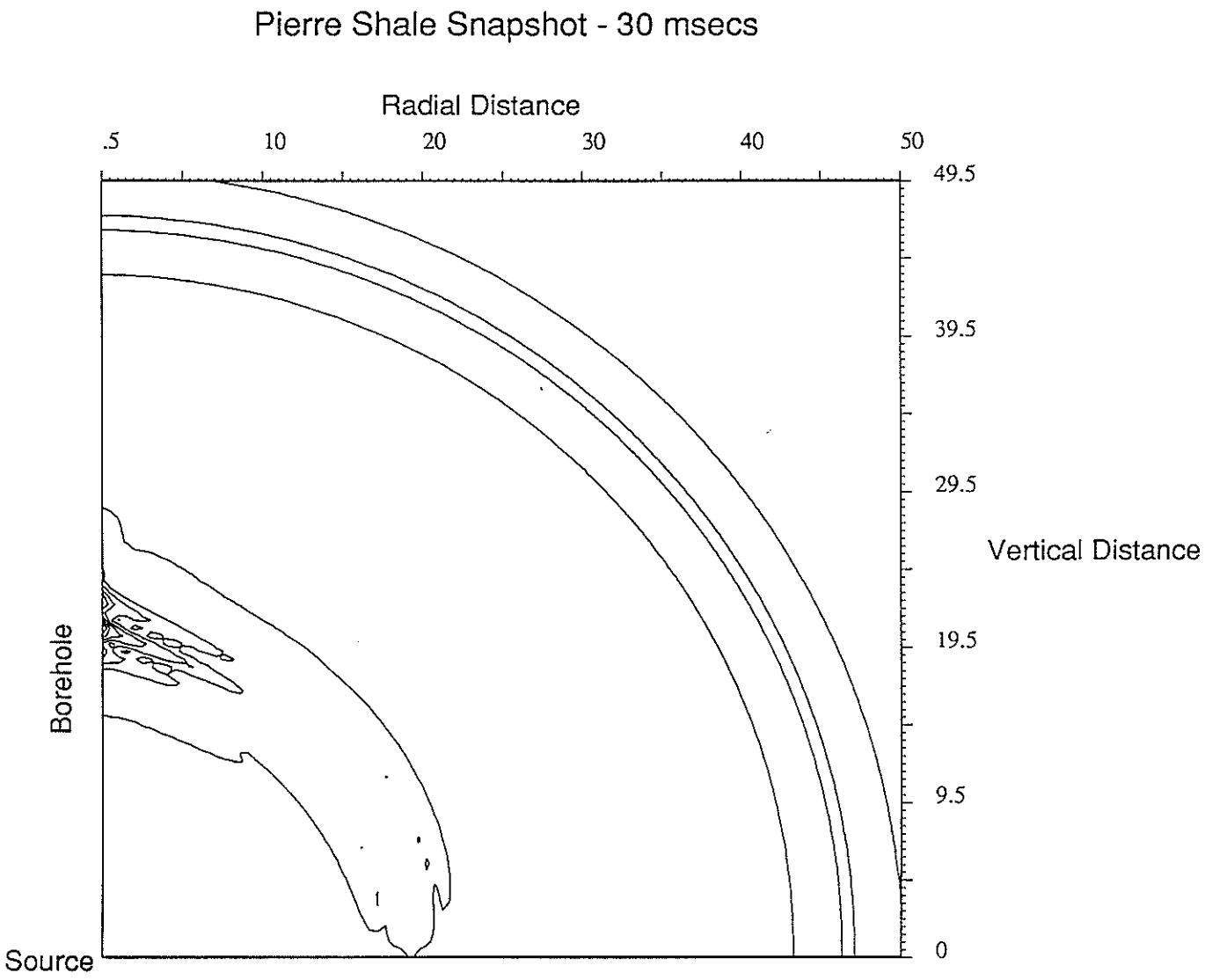

Figure 8: B) A snapshot at 30 msecs of total displacement calculated on a 50 m by 50 m grid and contoured. Same model as part A. Notice constructive interference of tube wave is moving away from the borehole and has maintained its shape.

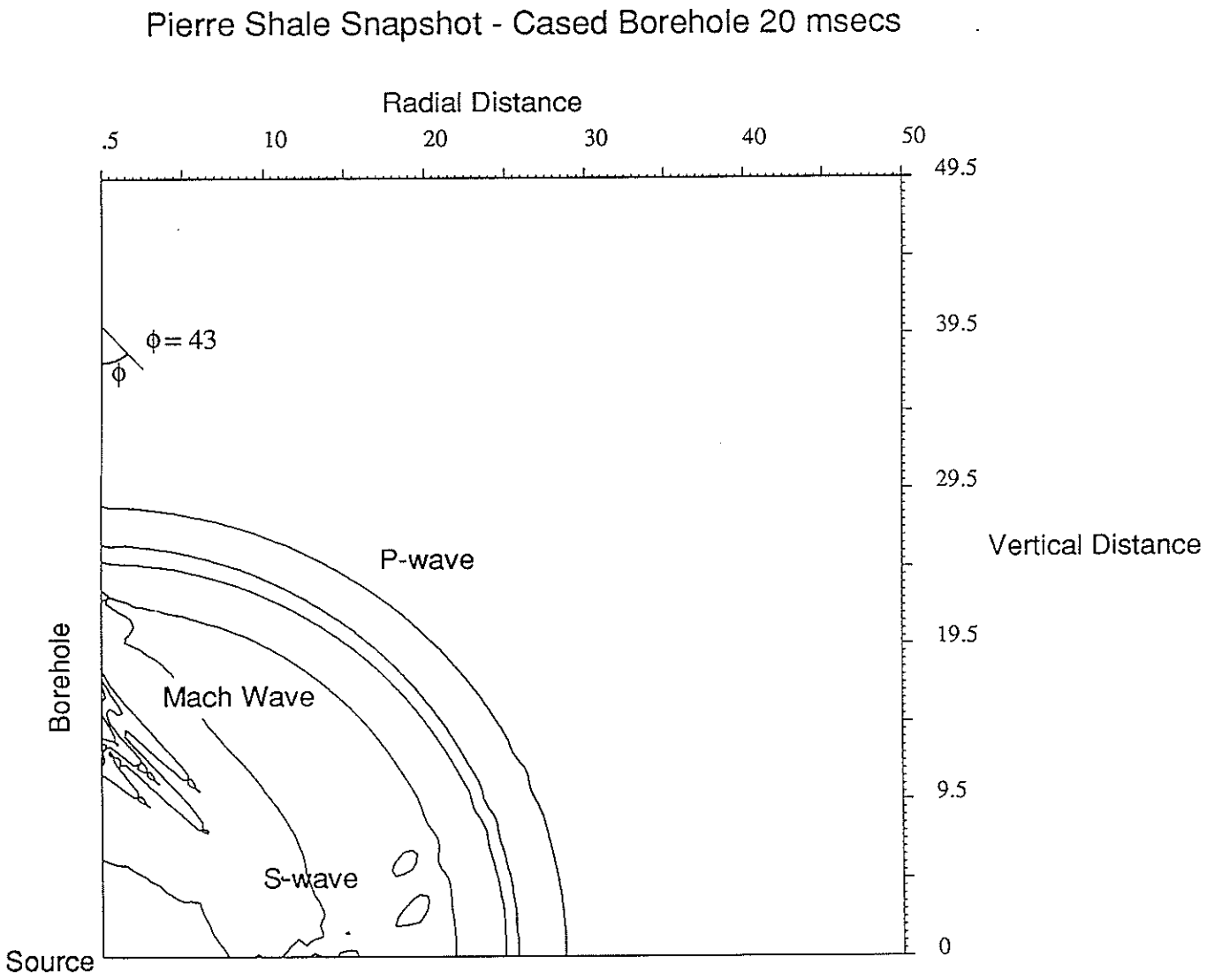

Figure 9: A snapshot at 20 msecs of total displacement calculated on a 50 m by 50 m grid and contoured. Origin is source point in lower left hand corner. Velocities and densities for this model are those of Pierre Shale. However, a 0.5 cm layer of casing has been inserted into the model increasing the tube wave velocity and causing a shallower and thus more prevalent Mach angle. Again notice tube wave emitting energy that is constructively interfering. 200 Hz Ricker wavelet. Contours: minimum 1×10^{-5}, maximum 4.01×10^{-3}, interval 1×10^{-3}.

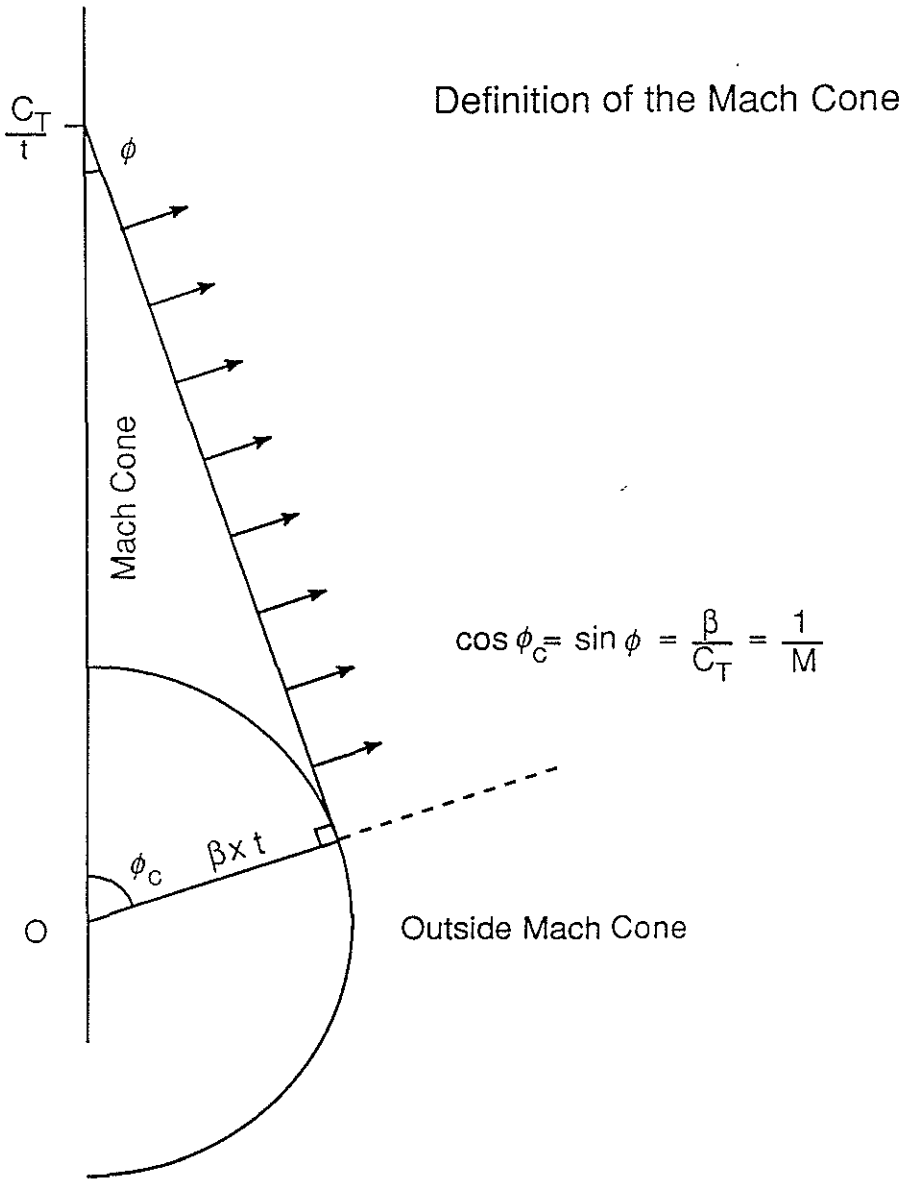

Figure 10: Geometry of Mach wave and Mach cone. As wavefield travels away from the borehole there are three parts. The up and downgoing tube waves and the outward central disturbance. The constructive interference does not begin until the tangent intersects the circle at ϕ_c. Anything within this tangent is said to be in the Mach cone. The central disturbance is outside the Mach cone. When the shear wave velocity is close to the tube wave velocity but still less than it, most of the radiation will be outside the Mach cone.

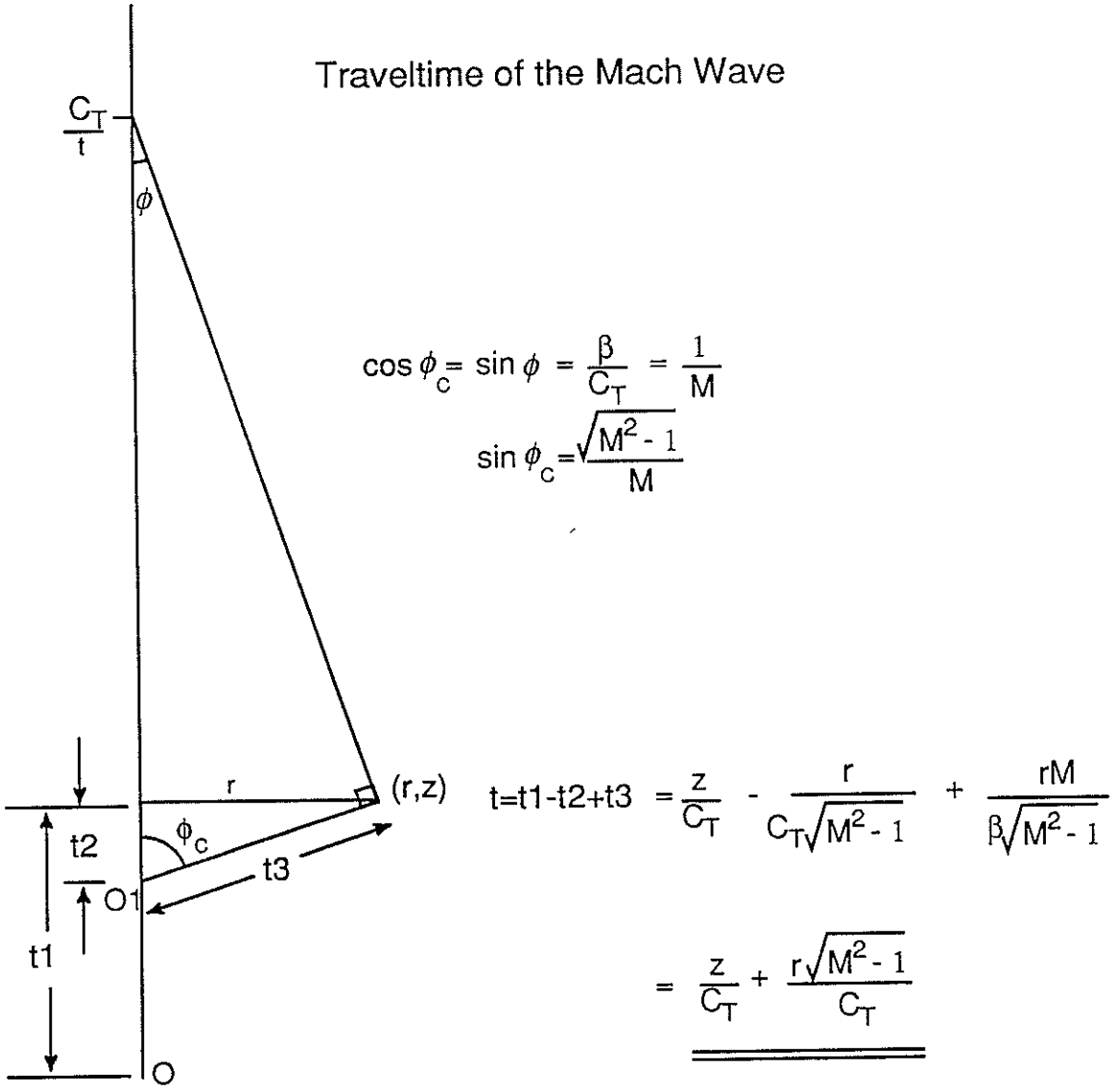

Figure 11: This figure illustrates the hybrid nature of the Mach wave travel time. When an observation point is inside the Mach cone the travel time will consist of the time to travel to point 01 at tube wave velocity and the time to travel from 01 to the observation point at shear wave velocity. This hybrid travel time is given by the formula $\frac{z}{C-T} + \frac{r\sqrt{M^2-1}}{C_T}$ (Ben-Menahem and Singh, 1987) after simplification.

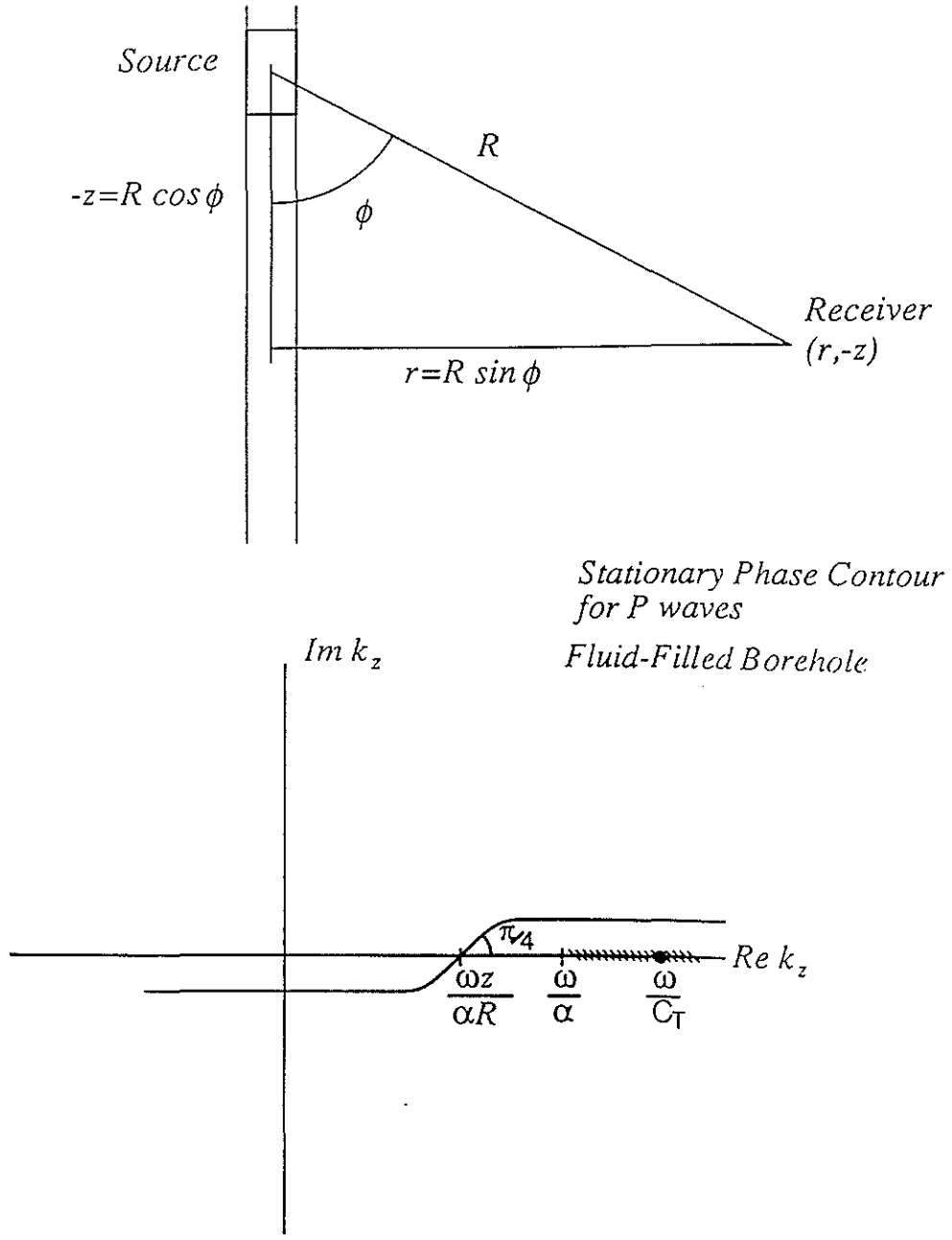

Figure 12: Top half is geometry used to evaluate stationary phase contours. Bottom half is stationary phase contour for P waves. The quantity $\frac{\omega z}{\alpha R}$ will range between 0 and $\frac{\omega}{\alpha}$. Assuming $C_T < \alpha$, which is valid for most rocks, the tube wave pole will not be intersected and the branch cut will have little effect.

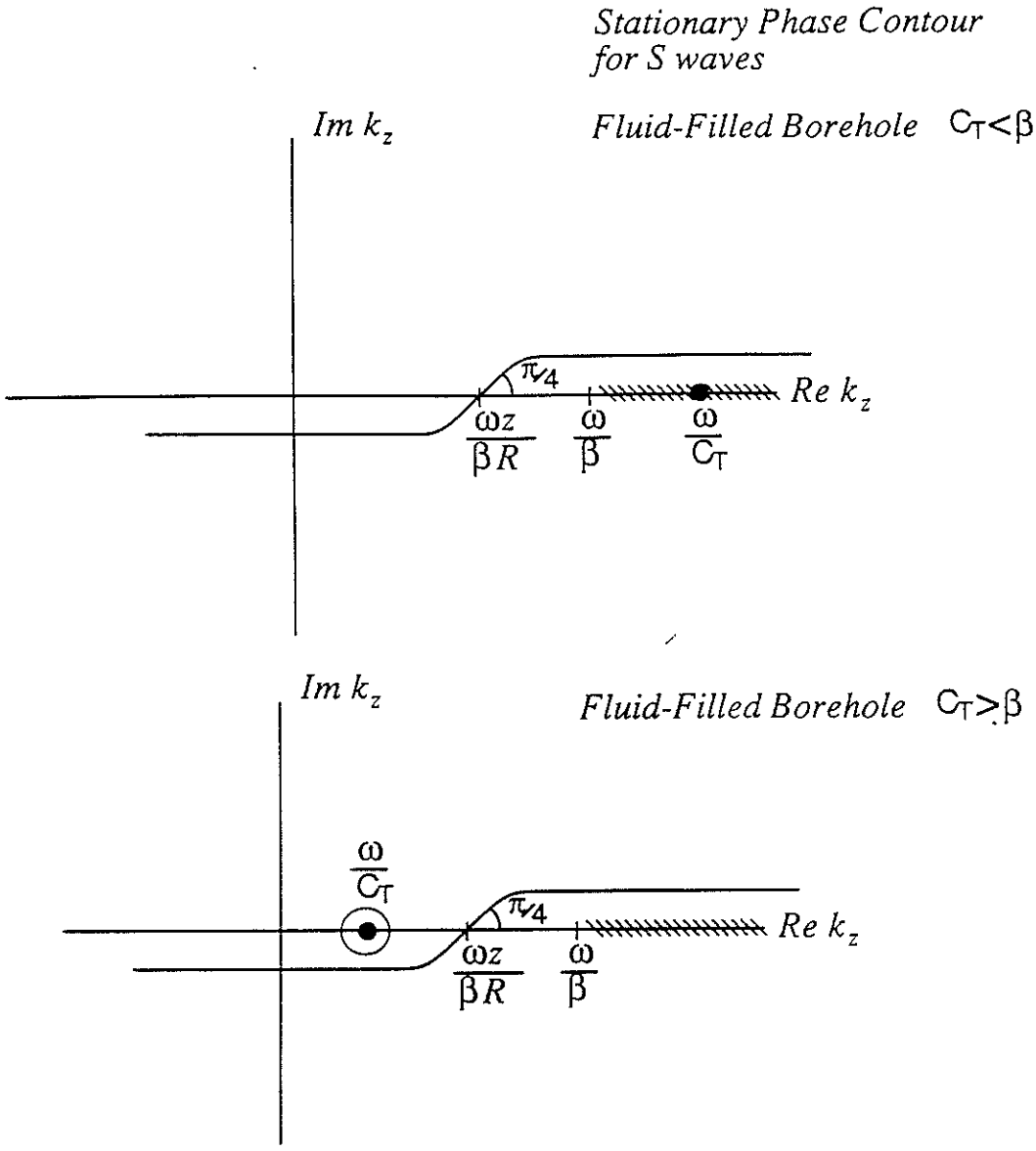

Figure 13: Stationary phase contours for S wave for sub-shear case top and super-shear case bottom, geometry is same as last figure. Sub-shear case where tube wave velocity is less than shear wave velocity is very similar to previous figure for P waves. However when $C - T > \beta$, tube wave pole is to left of branch cut and stationary phase contour will intersect pole with pathologic effects. Mach cone region is in between pole and $\frac{\omega}{\beta}$.

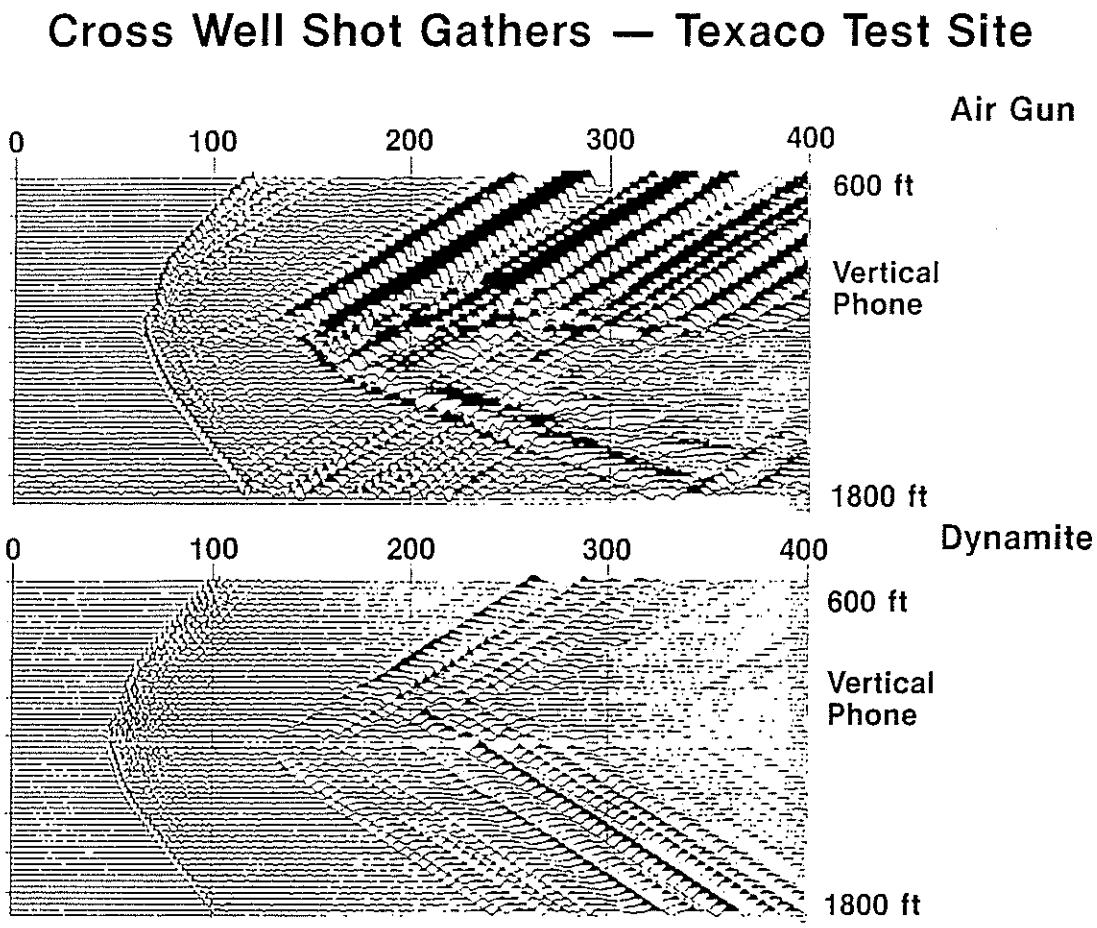

Figure 14: Data example. Group shoot at Texaco's Humble test site. Receiver array is buried with no receiver borehole. High amplitude arrivals for both air gun and dynamite do not exhibit hyperbolic moveout expected of shear waves. In fact, these arrivals are Mach waves. Because dynamite produces less tube wave energy in proportion to P waves than the airgun, the Mach waves are relatively smaller for the dynamite.